2019 2nd IEEE International Conference on Soft Robotics (RoboSoft)
COEX, Seoul, Korea, April 14-18, 2019

Dimension Optimization of Pneumatically Actuated Soft Continuum Manipulators

Xiangyu Peng[1], Ningbin Zhang[1], Lisen Ge[1] and Guoying Gu[1,2,*]

***Abstract*— Soft continuum manipulators exhibit promising applications over traditional rigid manipulators because of their compliant bodies. However, the unexpected phenomenon due to the gravity, called *instability*, makes it challenging for design, modeling and control. In this paper, we design a two-section pneumatically actuated soft continuum manipulator, containing three-chambered pneumatic actuators in each section and investigate the optimal Length to Diameter Ratio (LDR) of the manipulator by Finite Element Analysis (FEA). We introduce a new measure variable — workspace ratio (WR) — to examine the workspace as well as the *instability* and we can determine our optimal LDR value based on this variable. A soft manipulator is then fabricated and experimentally tested. The experimental results are in good agreement with model simulation. Results show the optimal value of LDR is at the maximum LDR, which is about 4.71 for one-section soft manipulator and 3.91 for two-section soft manipulator. This can be the guidance to the multiple-section soft manipulator design for further applications.**

I. INTRODUCTION

Discrete hyper-redundant manipulators are widely used especially where repetitive tasks are needed [1] [2]. Nonetheless, when interacting with human, the rigid components and large weight lead to safety problems. Meanwhile, with the concept of soft robotics [3] [4], manipulators made of soft materials can serve as a better alternative because of its light-weight, compliant mechanics and high power-to-weight ratios [5]–[7]. Soft continuum manipulators are generally classified into three categories according to their actuation methods: cable-driven soft manipulators [8] [9], pneumatically actuated soft manipulators [10] [11] and hybrid soft manipulators [12] [13]. As one of the most common types, pneumatically actuated soft continuum manipulators are promising in several fields, such as the STIFF-FLOP surgical manipulator used for minimal access surgery [14] [15], modular soft robotic wrist applied to underwater manipulation [16] and soft robotic arm for adaptable grasping [17].

An important reason limiting the widespread use of soft continuum manipulators is its limited workspace. Many recent works start to investigate the workspace of soft manipulators. Modeling approaches [18] are popular as they can numerically calculate the workspace. Camera tracking systems [19] [20] provide a more convenient alternative for rough computation. However, both these methods are used to calculate the workspace after design and fabrication and parameters are chosen relying on intuition only.

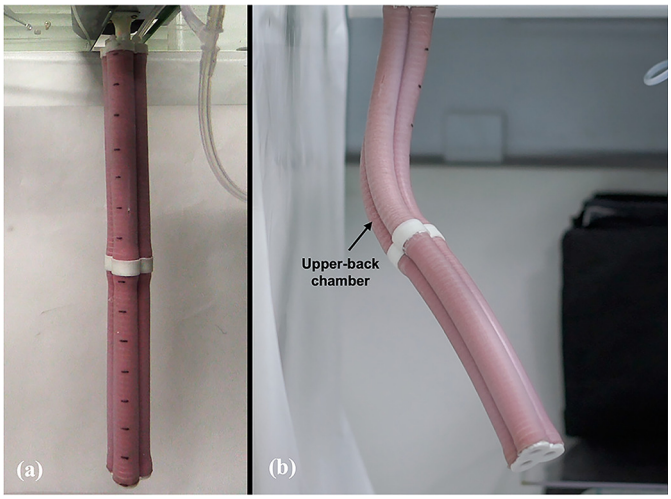

Fig. 1. Soft continuum manipulator. (a) At rest state. (b) The configuration of the soft manipulator when upper-back chamber reaches the air pressure of 160kPa.

Previous researches have also explored some related influence factors on the manipulator workspace. Nguyen et al. [21] developed a Soft Poly-Limbs and investigated the influence of several related parameters (ring count, ring thickness, taper ratio and spacing between actuators) on the manipulator's extension and bending angle in one section of SPL, but their effects on the workspace and payload capacity remains unclear. Gong et al. [22] carried out some works on the workspace simulation of multi-sections soft manipulator and found two-section soft arm reached more accessible space than one-section arm. Force-output of actuators and weight of soft manipulators could significantly limit the reachable envelop of soft manipulators [23]. Cianchetti et al. [14] found that increasing stiffness of the manipulator could lead to larger workspace. The combination of various cross-sectional technologies on Bionic Handling Assistant of Festo Co. [24] also led to a larger workspace. Many design strategies and structure parameters are explored in previous works, however, they all lack a more quantitative relation: to what extent do these strategies and parameters influence the workspace of soft manipulators.

In this paper, we focus on one of these parameters –

*This work was partially supported by the National Natural Science Foundation of China (grant nos. 51622506 and 91848204) and the Science and Technology Commission of Shanghai Municipality (grant no. 16JC1401000).

[1] Soft Robotics and Biodesign Lab, Robotics Institute, School of Mechanical Engineering, Shanghai Jiao Tong University, Shanghai 200240, China
[2] State Key Laboratory of Mechanical System and Vibration, Shanghai Jiao Tong University, Shanghai 200240, China
*Corresponding author: Guoying Gu (guguoying@sjtu.edu.cn).

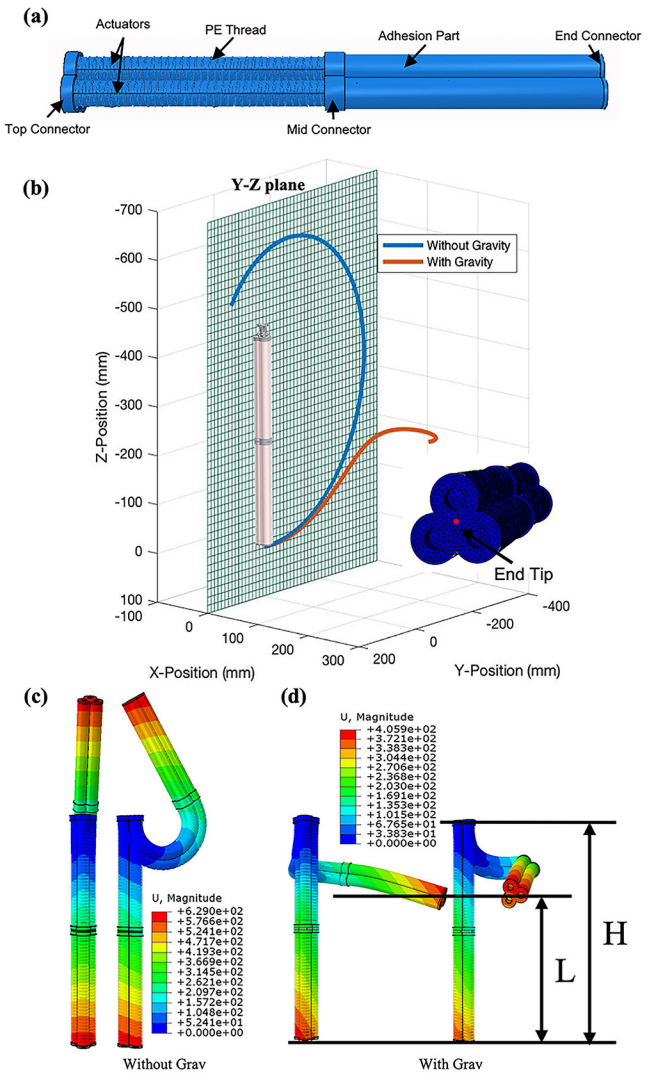

Fig. 2. FEA results comparison between manipulation with gravity and without gravity. (a) FEA model for soft manipulator, including six fiber-reinforced pneumatic actuators, two adhesion parts and top/mid/end connector. (b) End tip trajectory with/without gravity. Green mesh is the Y-Z plane. (c) FEA result with gravity. (c) FEA result without gravity. (H is the original length of soft manipulator. L is the largest vertical displacement of the end tip under gravity).

Length to Diameter Ratio (LDR), and study its effect on the behavior of soft manipulators. We investigate how the change of LDR affects the workspace ratio (WR) of one-section and two-section soft manipulators through Finite Element Analysis (FEA). Through the WR and LDR curves we can find the optimal LDR and this value enables each manipulator to achieve the maximum WR and minimize the effect of gravity. We then fabricate a two-section soft manipulator to verify the FEA results. Experimental results of the configuration of the soft manipulator match well with FEA results. FEA results can then be used to predict the trend of WR as LDR changes. The results of this work can shed light on the design of soft continuum manipulators in the future and provide reference for more applications.

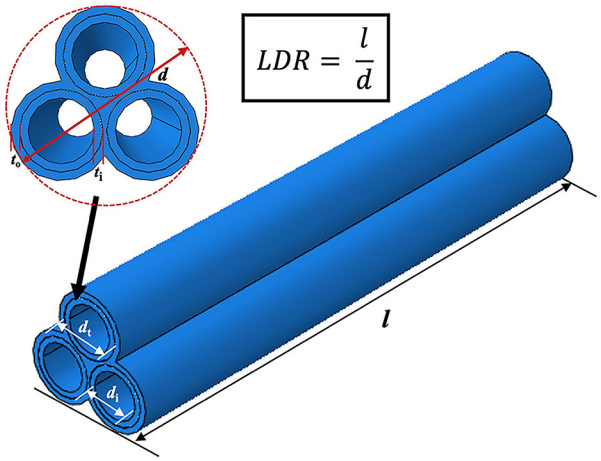

Fig. 3. The structure of one section of the soft manipulator and its related parameters.

II. INSTABILITY PHENOMENON

For a multiple-section soft manipulator as shown in Fig. 1 (b), a twisting phenomenon usually occurs when we actuate the upper-back chamber although few study reports it. This phenomenon prevents the soft manipulator from reaching a larger workspace, as its end tip moves laterally rather than upward when the air pressure reaches a certain value. Its highest reachable position is severely limited. We call this phenomenon *instability*. To find out the reason of it and avoid this phenomenon, we use Finite Element Analysis (FEA) to study this behavior numerically.

The models of soft manipulators are designed and assembled in Solidworks 2016 (Dassault System, S.A), including six fiber-reinforced pneumatic actuators, two adhesion parts and a top/mid/end connector (Fig. 2(a)). The FEAs are carried out using ABAQUS 6.14-4 (Dassault System, S.A.). Since the soft manipulator is designed to carry objects, whether through whole arm grasping or adding end effector, the manipulators should be set to a high shore hardness to provide enough force. By comparing the hardness of frequently-used silicone materials (Table I), we chose a relatively hard material for actuators and a quite soft material for adhesion, which is: Elastomer M4601 (Wacker Inc.) for actuators and Ecoflex 00-30 (Smooth-on Inc.) for adhesion parts. Hence, Yeoh model [25] (C10 = 0.11, C20 = 0.02) and Ogden model [26] ($\mu 1$ = 0.001887, $\alpha 1$ = -3.848, $\mu 2$ = 0.02225, $\alpha 2$ = 0.663, $\mu 3$ = 0.003574, $\alpha 3$ = 4.225, D1 = 2.93, D2 = D3 = 0) are employed for actuators and adhesion parts in the FEA model. A linear-elastic model is used for the fiber (E = 31067MPa, μ = 0.36). Both actuators and adhesion parts are meshed in C3D4H elements. For the polyethylene (PE) thread the element type is set to be B32. The element sizes are 2.5 for actuators, adhesion parts, connectors and 1 for PE thread. We add uniformly distributed inner pressure to upper-back chamber with the magnitude of 300kPa. Gravity is applied to one model and removed from the other.

We set the initial position of the soft manipulator end tip

TABLE I

HARDNESS OF COMMON SILICONE MATERIALS

Silicone Material	Shore Hardness
Ecoflex 00-XX	00-XX (XX = 10, 20, 30, 35, 50)
Dragon Skin YY	A-YY (YY = 10, 20, 30)
Elastomer M4601	A-28

as (0,0,0) and plot its trajectory as air pressure increases. Results show large difference between models with and without gravity (Fig. 2 (b)). The motion trajectory deviates from Y-Z plane under gravity. In addition, it limits displacement in Z direction, which means a great reduction in manipulator's workspace. From the comparison, we can conclude that gravity has a dramatic influence on soft manipulator, mainly because of the compliant mechanism of soft materials. Also, there is no manufacturing errors or assembly errors in FEA simulation, which proves that the instability is not due to the error amplification under large pressure.

III. OPTIMIZATION

Several structure parameters of this kind of design can influence the workspace of manipulators, like taper ratio of each segment [22], actuator thickness [21] and cross-sectional area [24]. In this paper, we mainly focus on the influence of Length to Diameter Ratio (LDR, illustrated in Fig. 3) on soft manipulator's workspace. This is a parameter most closely related to the size of the whole object and is usually the first parameter to be determined when designing. Therefore, it is critical to find out its optimal value. To investigate the influence of LDR, other geometry parameters in simulation are fixed as follow (Fig. 3): the actuator outer diameter d_t = 15mm, the actuator inner diameter d_i = 11mm, the actuator thickness t_i = 2mm, the adhesion part thickness t_o = 3mm. Since three actuators are tangent to each other, we can calculate the diameter of each section d = 38.32mm. The section length is l.

Here we provide a new variable as the measure of the workspace of soft manipulator: The ratio between the largest vertical displacement of the end tip with gravity (L) and the original length of the soft manipulator (H). We call it *workspace ratio* (WR).

$$workspace\ ratio\ =\ L\ /\ H \tag{1}$$

Parameter L and H are illustrated in Fig. 2 (d).

The reasons we use WR are as follow. First, the three-dimensional workspace is rarely possible to calculate using FEA. We have to run lots of trials to get enough statistics for one situation, which takes infinite time. Second, one-dimensional figure is much easier to compare than three-dimensional surface because it is very intuitive. Since *instability* is caused by gravity and the direction of gravity is constant, i.e., one dimensional, hence a one-dimensional variable is enough to measure the influence of gravity.

By dividing the original length, we are able to compare the proportion of the ideal workspace the soft manipulator can actually cover. The larger proportion it can reach, the better it is and the less influence it suffers from *instability*.

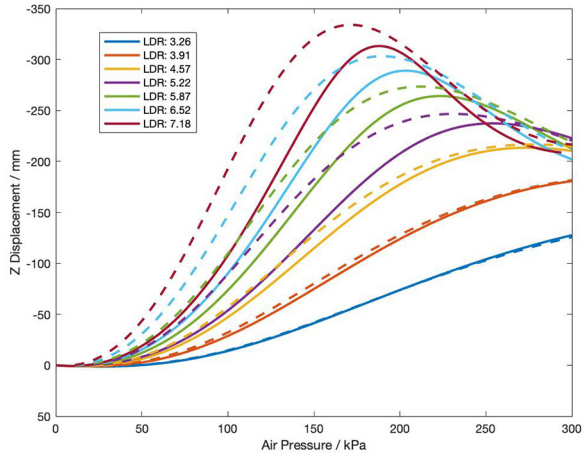

Fig. 4. The relationship between air pressure in one actuator and the vertical displacement of the end tip of soft manipulator. The dotted line is FEA without gravity and the solid line is with gravity.

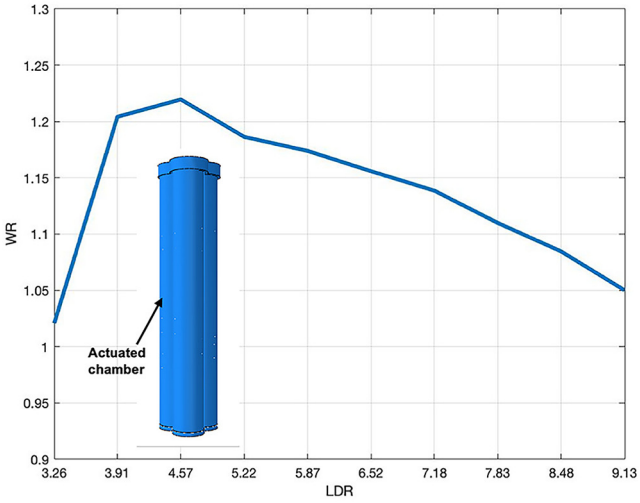

Fig. 5. The WR varies as LDR changes. From the figure we can see the maximum WR and its corresponding LDR value.

A. One-Section Soft Manipulator

We first execute FEA simulation on one-section soft manipulator. The section length changes from 125mm to 350mm with an increment of 25mm. In this sense, we vary the LDR from 3.26 to 9.13.

Based on experiments, we set 300kPa as the maximum air pressure for the actuator, because the silicone adhesion has a limited bearing capacity. According to the simulation result, as shown in Fig. 4, the critical value (the air pressure when the end tip of soft manipulator reaches the highest position) decreases as the length of the section increases. We can see that when LDR is smaller than 3.91, it doesn't get to its highest position before the air pressure reaches 300kPa. Therefore, it's not effective because we cannot fully utilize its deformation. On the other side, as the LDR increases, the

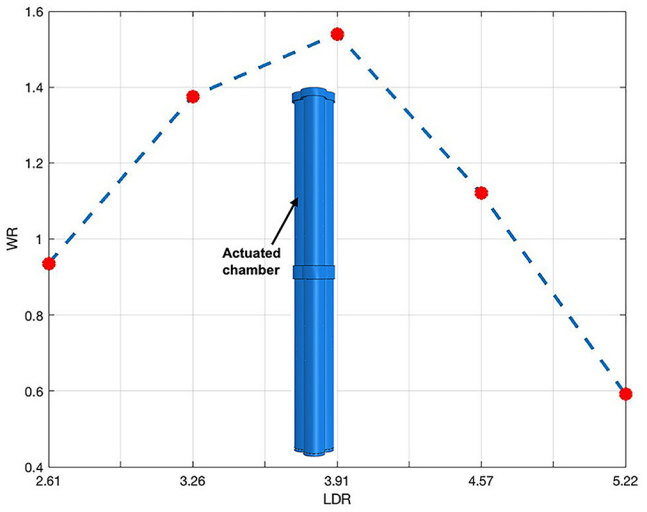

Fig. 6. The relationship between air pressure in upper-back chamber and the vertical displacement of the end tip of soft manipulator.

end tip reaches the highest position with smaller air pressure. This is because soft manipulator with large LDR is easier to be influenced by gravity. Also, we can see from Fig. 5 that as the LDR increases, the deviation becomes greater between the dotted line (without gravity) and the solid line (with gravity), which proves greater influence on large LDR. And the optimal choice for a section is around 4.57, which is 150mm in length.

B. Two-Section Soft Manipulator

To extend the design into multiple-section soft manipulator, we execute FEA simulation for a two-section manipulator. We inflate the upper-back chamber and the result is shown in Fig. 6.

We can see that the trend is similar to that of one-section soft manipulator, where there is a peak value. Therefore, there is still an optimal choice for two-section manipulator. However, as we can see from the plot, the peak appears when LDR is around 3.91, which is less than 4.57, the optimal value for one-section soft manipulator. This change is due to the addition of the second section which is not actuated but introduces additional weight to the whole model.

IV. EXPERIMENTAL VERIFICATION

A. Soft Manipulator Fabrication

There are four steps to manufacture a single section of the soft manipulator as shown in Fig. 7. First, we need to assemble 5 mold parts, including two parts with helical extrudes features. The imprinted helix curve helps the winding of fibers to limit the radial expansion. The round rod helps shape the hallow central cavity. The top/end cap ensure the desired concentricity within the mold. The molds in this fabrication are all 3D printed. Then, we pour silicone (M4601, Elastosil) into the mold and put it in the oven at 50°C for 2 hours. Next, we demold the cured actuator and wind asymmetrical fibers around it. Two fibers are identical

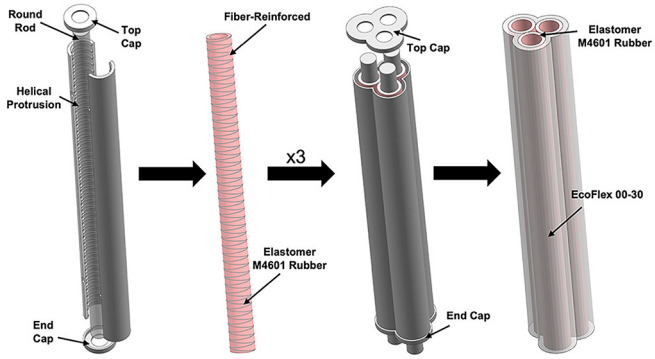

Fig. 7. Fabrication process of a section of soft manipulator. (a) Mold for a single actuator. (b) Fiber-reinforcement to limit radial expansion. (c) Mold for fusion to make a section. (d) Single section of a soft manipulator.

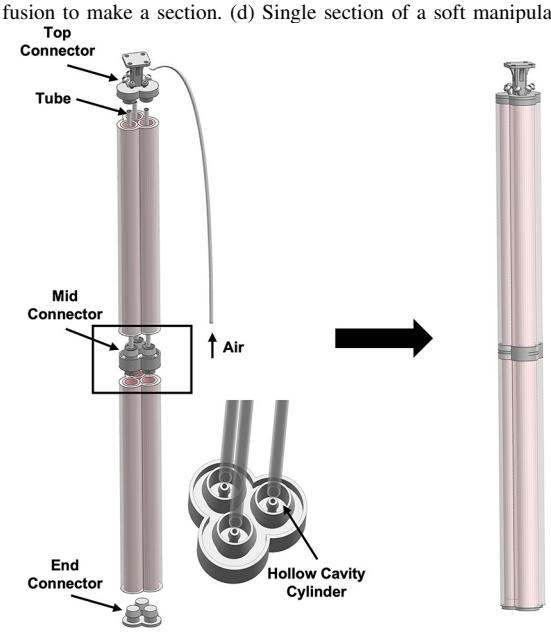

Fig. 8. Multi-Section assembly. (a) Sections joining and transmission tubes arrangement. (b) A two-section soft manipulator.

in pitch to ensure axial extension instead of bending. After repeating the first two steps twice, we assemble three actuators together, each tangent to another. The second curing process is similar to that of a single actuator. With less shore hardness than M4601, Ecoflex 00-30 adheres the three actuators as a whole. Then we join two sections to each side of the connector (Fig. 8) and seal the connection place using a silicone adhesive (RTV704, Ausbond).

The transmission tubes we use are also made of silicone rubber, with 4mm of inner diameter and 0.5mm in thickness. Since it is easy for tubes to burst out when the air pressure is too high, we pour Ecoflex 00-30 silicone rubber in the hollow cavity cylinder of the connector, helping increase its firmness in connection. This method contains tubes inside the soft manipulator, making it far simpler in shape.

B. Experimental Validation

To verify the FEAs result, we conduct experimental tests on the two-section soft manipulator with 220mm long of

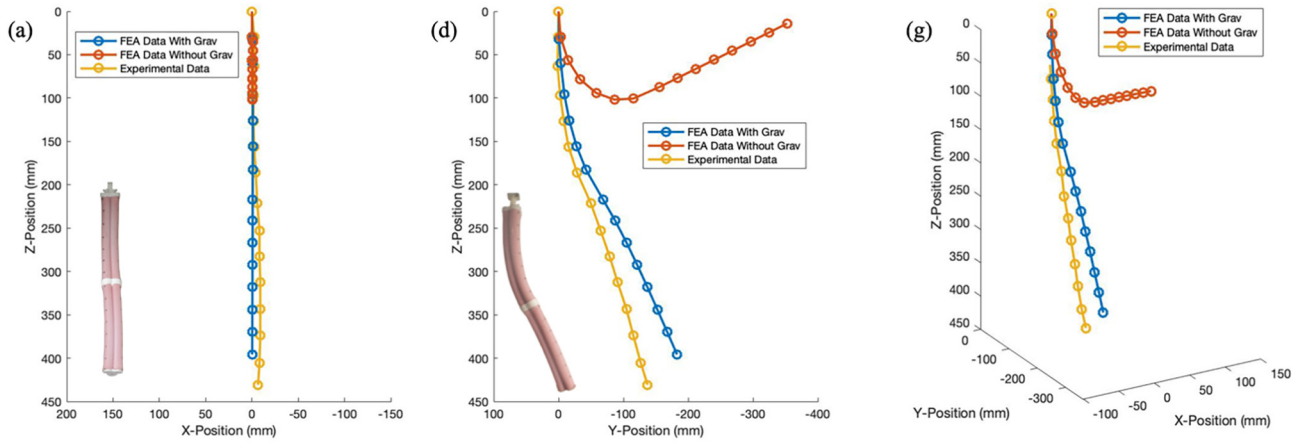

Fig. 9. FEA results with/without gravity and experimental test results of the configurations of soft manipulator with air pressure in upper-back chamber in 100kPa, 150kPa and 200kPa. (a) – (f) show the configurations of soft manipulator in XY-plane and YZ-plane. (g) – (i) show the configurations of soft manipulator in 3D-space.

each section. We apply pressured air into the upper-back chamber up to 100kPa, 150kPa and 200kPa, respectively. We fix the soft manipulator on its top connector side and set the end tip free as we set in FEA. We set up a two-camera system to capture the images synchronously, with one on side view (YZ-coordinates) and the other on front view (XZ-coordinates). By tracking markers drawn on soft manipulator (Fig. 9, markers are arranged vertically along

the manipulator and distributed every 30mm), we can get the relative coordinates of each marker by ImageJ (NIH). Then we use MATLAB (MathWorks) to transfer the relative coordinate of each marker into their actual coordinates in XZ- and YZ- format. By combining these two coordinates, we can get 3D coordinates of these markers. With this method, we plot the configuration of soft manipulator and reflect *instability* numerically.

As shown in Fig. 9, the *instability* becomes more and more obvious as the pressure increases. While some deviation existed in the second section due to the fabrication and assembly errors Experimental results of the configuration of the soft manipulator match well with FEA results in the first section when pressure is 100kPa and 150kPa. Therefore, FEA results can be used to calculate WR and the trend of WR as well as the optimal LDR. Experimental results and FEA results match well. This inconsistency may be caused by the nonlinear behavior, instability of the air source and errors in markers extraction. Finally, our results show that we provide the method by using the FEA simulation to aid the design of the multiple-section soft manipulator for further applications.

V. CONCLUSION

This paper presents a common phenomenon: the *instability* existing in soft manipulators and this phenomenon is closely related to a structure parameter, the Length to Diameter Ratio (LDR). Effects of LDR on the soft manipulator's behavior are analyzed in detail. A measure variable — workspace ratio (WR) — to evaluate the gravity influence and the workspace is defined and analyzed to better understand the influence of LDR. By using the FEA method, we calculate the WR under different LDRs. Results demonstrate that as the LDR increases, the WR rises at first due to the limit of maximum air pressure and decreases later due to the influence of gravity. We can obtain the optimal LDR values for one-section soft manipulator and two-section soft manipulator as around 4.57 and 3.91 respectively. This study can guide the design of soft manipulators, which broadens their applications in soft robotics.

REFERENCES

[1] Michael W Hannan and Ian D Walker. Kinematics and the implementation of an elephant's trunk manipulator and other continuum style robots. *Journal of robotic systems*, 20(2):45–63, 2003.

[2] Rob Buckingham. Snake arm robots. *Industrial Robot: An International Journal*, 29(3):242–245, 2002.

[3] Deepak Trivedi, Christopher D Rahn, William M Kier, and Ian D Walker. Soft robotics: Biological inspiration, state of the art, and future research. *Applied bionics and biomechanics*, 5(3):99–117, 2008.

[4] Guoying Gu, Jiang Zou, Ruike Zhao, Xuanhe Zhao, and Xiangyang Zhu. Soft wall-climbing robots. *Science Robotics*, 3(25):eaat2874, 2018.

[5] Guoying Gu, Jian Zhu, Li-Min Zhu, and Xiangyang Zhu. A survey on dielectric elastomer actuators for soft robots. *Bioinspiration & biomimetics*, 12(1):011003, 2017.

[6] Daniela Rus and Michael T Tolley. Design, fabrication and control of soft robots. *Nature*, 521(7553):467, 2015.

[7] Carmel Majidi. Soft robotics: a perspective—current trends and prospects for the future. *Soft Robotics*, 1(1):5–11, 2014.

[8] Ian A Gravagne and Ian D Walker. Uniform regulation of a multi-section continuum manipulator. In *Robotics and Automation, 2002. Proceedings. ICRA'02. IEEE International Conference on*, volume 2, pages 1519–1524. IEEE, 2002.

[9] Michele Giorelli, Federico Renda, Marcello Calisti, Andrea Arienti, Gabriele Ferri, and Cecilia Laschi. A two dimensional inverse kinetics model of a cable driven manipulator inspired by the octopus arm. In *Robotics and Automation (ICRA), 2012 IEEE International Conference on*, pages 3819–3824. IEEE, 2012.

[10] Michael B Pritts and Christopher D Rahn. Design of an artificial muscle continuum robot. In *Robotics and Automation, 2004. Proceedings. ICRA'04. 2004 IEEE International Conference on*, volume 5, pages 4742–4746. IEEE, 2004.

[11] Rongjie Kang, David T Branson, Tianjiang Zheng, Emanuele Guglielmino, and Darwin G Caldwell. Design, modeling and control of a pneumatically actuated manipulator inspired by biological continuum structures. *Bioinspiration & biomimetics*, 8(3):036008, 2013.

[12] Inderjeet Singh, Yacine Amara, Achille Melingui, Pushparaj Mani Pathak, and Rochdi Merzouki. Modeling of continuum manipulators using pythagorean hodograph curves. *Soft robotics*, 2018.

[13] Michael D Grissom, Vilas Chitrakaran, Dustin Dienno, Matthew Csencits, Michael Pritts, Bryan Jones, William McMahan, Darren Dawson, Chris Rahn, and Ian Walker. Design and experimental testing of the octarm soft robot manipulator. In *Unmanned Systems Technology VIII*, volume 6230, page 62301F. International Society for Optics and Photonics, 2006.

[14] Matteo Cianchetti, Tommaso Ranzani, Giada Gerboni, Iris De Falco, Cecilia Laschi, and Arianna Menciassi. Stiff-flop surgical manipulator: mechanical design and experimental characterization of the single module. In *Intelligent Robots and Systems (IROS), 2013 IEEE/RSJ International Conference on*, pages 3576–3581. IEEE, 2013.

[15] Matteo Cianchetti, Tommaso Ranzani, Giada Gerboni, Thrishantha Nanayakkara, Kaspar Althoefer, Prokar Dasgupta, and Arianna Menciassi. Soft robotics technologies to address shortcomings in today's minimally invasive surgery: the stiff-flop approach. *Soft robotics*, 1(2):122–131, 2014.

[16] Shunichi Kurumaya, Brennan T Phillips, Kaitlyn P Becker, Michelle H Rosen, David F Gruber, Kevin C Galloway, Koichi Suzumori, and Robert J Wood. A modular soft robotic wrist for underwater manipulation. *Soft robotics*, 2018.

[17] Zhe Chen, Xueya Liang, Tonghao Wu, Tenghao Yin, Yuhai Xiang, and Shaoxing Qu. Pneumatically actuated soft robotic arm for adaptable grasping. *Acta Mechanica Solida Sinica*, pages 1–15.

[18] Bryan A Jones and Ian D Walker. Kinematics for multisection continuum robots. *IEEE Transactions on Robotics*, 22(1):43–55, 2006.

[19] Lisen Ge, Longteng Dong, Dong Wang, Qi Ge, and Guoying Gu. A digital light processing 3d printer for fast and high-precision fabrication of soft pneumatic actuators. *Sensors and Actuators A: Physical*, 273:285–292, 2018.

[20] Tianyu Wang, Lisen Ge, and Guoying Gu. Programmable design of soft pneu-net actuators with oblique chambers can generate coupled bending and twisting motions. *Sensors and Actuators A: Physical*, 271:131–138, 2018.

[21] Pham Huy Nguyen, Curtis Sparks, Sai G Nuthi, Nicholas M Vale, and Panagiotis Polygerinos. Soft poly-limbs: Toward a new paradigm of mobile manipulation for daily living tasks. *Soft robotics*, 2018.

[22] Andrew D Marchese and Daniela Rus. Design, kinematics, and control of a soft spatial fluidic elastomer manipulator. *The International Journal of Robotics Research*, 35(7):840–869, 2016.

[23] Zheyuan Gong, Zhexin Xie, Xingbang Yang, Tianmiao Wang, and Li Wen. Design, fabrication and kinematic modeling of a 3d-motion soft robotic arm. In *Robotics and Biomimetics (ROBIO), 2016 IEEE International Conference on*, pages 509–514. IEEE, 2016.

[24] Andrzej Grzesiak, Ralf Becker, and Alexander Verl. The bionic handling assistant: a success story of additive manufacturing. *Assembly Automation*, 31(4):329–333, 2011.

[25] Panagiotis Polygerinos, Stacey Lyne, Zheng Wang, Luis Fernando Nicolini, Bobak Mosadegh, George M Whitesides, and Conor J Walsh. Towards a soft pneumatic glove for hand rehabilitation. In *Intelligent Robots and Systems (IROS), 2013 IEEE/RSJ International Conference on*, pages 1512–1517. IEEE, 2013.

[26] Gunjan Agarwal, Nicolas Besuchet, Basile Audergon, and Jamie Paik. Stretchable materials for robust soft actuators towards assistive wearable devices. *Scientific reports*, 6:34224, 2016.